Torque Improvement for Modified Double Stator Switched Reluctance Machines

Zhong Gao
Dept. of Mechanical Engineering
University College London (UCL)
London, United Kingdom
zhong.gao.23@ucl.ac.uk

Alessandro Rossi
Dept. of Mechanical Engineering
University College London (UCL)
London, United Kingdom
alessandro.rossi.23@ucl.ac.uk

Yugesh Sundharam
Dept. of Mechanical Engineering
University College London (UCL)
London, United Kingdom
yugesh.sundharam.23@ucl.ac.uk

Yuxiao Li
Dept. of Mechanical Engineering
University College London (UCL)
London, United Kingdom
yuxiao.li.23@ucl.ac.uk

Zechen Ye
Dept. of Mechanical Engineering
University College London (UCL)
London, United Kingdom
zechen.ye.23@ucl.ac.uk

Haoran Jiang
Dept. of Mechanical Engineering
University College London (UCL)
London, United Kingdom
haoran.jiang.23@ucl.ac.uk

Siyuan Zhang
Dept. of Mechanical Engineering
University College London (UCL)
London, United Kingdom
siyuan.zhang.23@ucl.ac.uk

Pedram Asef
Dept. of Mechanical Engineering
University College London (UCL)
London, United Kingdom
pedram.asef@ucl.ac.uk

Shun Cai
Dept. of Mechanical Engineering
University College London (UCL)
London, United Kingdom
shun.cai@ucl.ac.uk

***Abstract*—This study advances the design of double stator switched reluctance machines (DSSRMs) by focusing on mitigating torque ripple to improve efficiency and promote broader application. The research undertakes a comprehensive literature review, establishes a baseline design, and employs iterative enhancements alongside advanced 2D and 3D model simulations using SolidWorks and ANSYS Maxwell software. Significant findings include a torque ripple reduction of up to 9%, an increase in peak torque, and optimised magnetic flux distribution, achieved through adjustments in rotor segment geometry and electromagnetic force balancing methods. The outcomes highlight the critical role of magnetic force analysis, 3D modelling, and dynamic testing in enhancing DSSRM performance, establishing a foundation for future optimisations in design and materials for environmental and operational sustainability.**

***Index Terms*—Double stator, torque ripple, switched reluctance machine (SRM), finite element analysis, efficiency optimisation**

I. Introduction

The dual stator switched reluctance machine (DSSRM) emerges as an innovation in the field of electric machine design. Building upon a switched reluctance machine (SRM), the DSSRM aims to address the limitations, in particular the torque ripple and low power density. This research incorporates a dual stator configuration to improve the performance of the machine with the enhancement of magnetic flux interactions. The machine volume is optimised to allow for improved slot copper filling (i.e., larger space to accommodate copper windings), and thus enhance the magnetic flux as well as output torque, leading to a comparable torque density with that of permanent magnet synchronous machines (PMSMs) [1].

A. The Importance of SRMs

The modern electric machine technologies mainly include induction machines (IM), PMSMs, SRMs, and other emerging machines. PMSMs are dominated in the tractive industry, although the technology is expensive and faces supply chain issues since they require rare earth materials with limited supply and increasing costs [2]. Meanwhile, the SRM technology is favoured for its simplicity, robustness, and cost-effectiveness, especially compared against PMSMs [3].

The SRMs have been widely adopted in various industries; however, the technology does face significant drawbacks, including issues related to noise, vibration, and inferior efficiency leading to lower torque and power densities [2]. The main shortfall of SRMs is the torque ripple phenomenon which causes jittering within the machine, making it less applicable to high speed traction applications.

B. Optimisation Approaches

An effective solution to improve the torque and power density of SRM is to adopt double stator and spare more space to allocate the winding, which is acknowledged as DSSRM [4]. With higher Ampere-turn excitation and doubly salient structure, magnetic saturation is present at the tip of the stator and rotor tooth of DSSRM. The local saturation tends to sacrifice the torque density and cause additional pulsating torque, which needs to be addressed properly.

In this work, a DSSRM topology is initially designed and modelled to establish a baseline performance benchmark and analyse electromagnetic behaviour. Identified issues are then

addressed using strategies proposed in [5] and [6]. The aim is to develop a new modified configuration with reduced torque ripple and mitigation towards local magnetic saturation, offering more satisfactory output performance.

II. Development Process of DSSRM

To undergo the analysis of the proposed improvements, an initial benchmark is selected to perform the performance analysis. An improved design is further developed with geometric optimisation on the basis of benchmark design. The machine structure is modelled with SolidWorks and the electromagnetic performance is analysed with commercial finite element analysis (FEA) software, ANSYS Maxwell.

A. Working Principle

The driving mechanics to generate torque is through the continuous excitation of diametrically opposite phases. Similar to an SRM, where during the excitation of a phase the current passes through four opposed outer and inner stator poles. Due to the minimum reluctance of the energised stator poles the rotor will align with the excited stator poles to generate torque [7]. The electromagnetic force, in essence, emerges from the interaction between the normal and tangential components of flux density determined using the Maxwell Stress Tensor (MST) method [7].

B. Torque Ripple Mitigation

The method of sequential excitation of phases introduces inherent limitations, notably the introduction of torque ripple which produces an uneven power curve causing jittering in the machine during operation thus greatly limiting the applicability of the design in tractive applications [8]. To enhance torque in certain operations, the method of shifting alternating rotor segments by an angle δ suggested in [5] is employed, as presented in Fig. 1. This adjustment changes the angle of the rotor gap between consecutive rotor poles alternatingly enlarging and reducing the angle. The relationship between torque and inductance change rate (dL/dθ) is shown in (1a). The ideal δ angle starts from a base value and is fine-tuned using iterative evaluation to minimise the torque ripple [5]. The torque ripple is defined by (1b):

$$t = \frac{1}{2} i^2 \frac{dL}{d\theta} \tag{1a}$$

$$T_{\text{ripple}}(\%) = \frac{T_{\text{max}} - T_{\text{min}}}{T_{\text{avg}}} \tag{1b}$$

C. Magnetic Saturation Alleviation

Magnetic saturation in the stator and rotor cores is present when the flux density hardly increases with the excitation of an external magnetic field. The magnetic saturation should be alleviated to take full utilization of magnetic material. To prevent saturation while keeping high flux density, rotor and stator geometries are optimised. With the substitution of sharp edges with rounded ends to spread magnetic flux more evenly, the peak density is reduced to mitigate the magnetic saturation. This approach balances maximising flux density with preventing saturation, being crucial for maintaining high efficiency in DSSRMs.

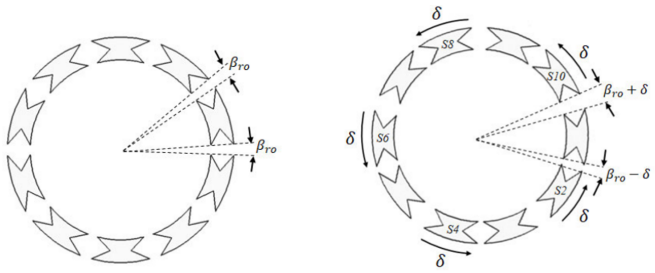

(a) Without segment shifts (b) With segment shifts

Fig. 1. Illustration of rotor segment shift [4]

D. DSSRM Topology and Design

The proposed topology is a 12-outer stator teeth/10-rotor segments/12-inner stator teeth, which is short for 12/10/12 configuration, with both the stator and rotor slot opening angles of 6° [9]. Using the relationship equations from [5] further angular dimensions are achieved to design an optimal 12/10/12 DSSRM with the specific aim of keeping the inner and outer slot areas equal to reduce radial motion. The rotor dimensions are determined using the dimensional relationship equations from [5], with the geometry of the rotor design after the proposed optimal design from [4] using a high degree of lamination which quantifies the number of layers used to construct the rotor geometry. A high degree is required to construct more complex rotor geometries.The remaining dimensions required are derived from the 12/10/12 DSSRM schematic from [9]. This is conducted to provide validation of the initial results of our benchmark design with the determined dimensions defined by TABLE I where the slot filling factor is 50%.

TABLE I
Benchmark DSSRM Dimensions

Dimension	Value (mm)
Axial length	84
Stator outer diameter	290
Air gap length	0.75
Inner diameter	80
Height of yoke	10
Height of inner stator	45
Height of outer stator	18.5

Having determined the required dimensions for the 12/10/12 DSSRM the cross section could then be constructed in a 2D space. This allowed for the boss extrusion of the cross section into 3D space to more accurately analyse the real working conditions of the electric machine, seen in Fig. 2. Copper windings can be modelled in ANSYS Maxwell for both 2D and 3D configurations. For 3D modelling, an orthogonal cross-section is utilised to meet the 50% slot fill factor requirement cited in [9]. Optimisation strategies mentioned in the study

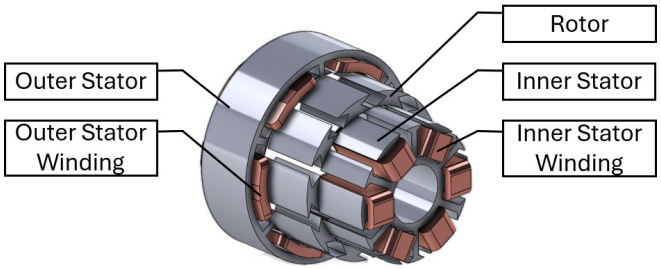

Fig. 2. 3D structure of DSSRM

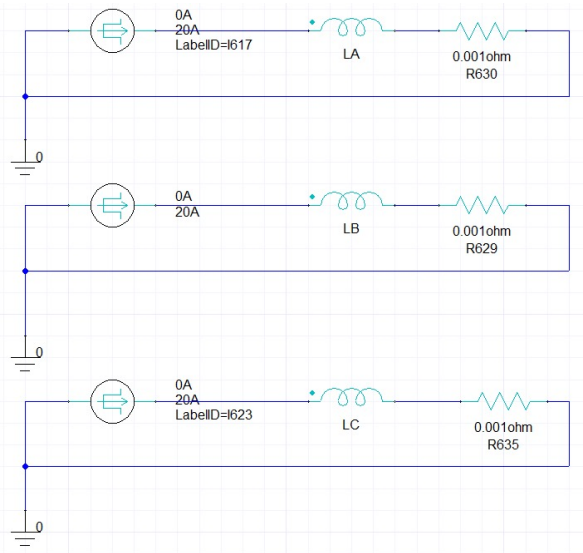

Fig. 3. Three phase excitation circuit

are then integrated to assess their effectiveness in enhancing baseline performance.

E. Electromagnetic Performance Evaluation

The electromagnetic evaluation is conducted using FEA on Ansys Maxwell. Transient calculations are performed to analyse the operating conditions of the DSSRM. To achieve this, an excitation circuit is necessary for proper sequential excitation of the phases. A 120° unipolar excitation pattern is implemented to produce high torque/power density [10]. To implement this current waveform a circuit structure is constructed as demonstrated in Fig. 3 with the excitation current produced shown in Fig. 4.

F. Electromagnetic Force Analysis

The electromagnetic force arises from the interaction of normal and tangential force components. This relationship is given by (2) [6].

$$f_{\text{normal}} = \frac{1}{2\mu_0}(B^2_{\text{normal}} - B^2_{\text{tangential}}) \tag{2a}$$

$$f_{\text{tangential}} = \frac{1}{2\mu_0}(B^2_{\text{normal}} \times B^2_{\text{tangential}}) \tag{2b}$$

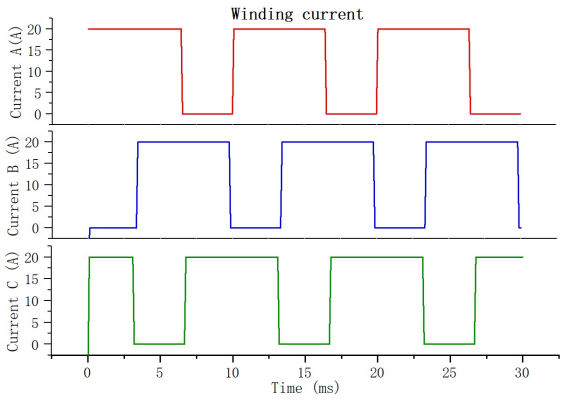

Fig. 4. Three phase excitation current

III. Electromagnetic Performance Analysis

In this section, the results of electromagnetic performance for both 2D and 3D FEA models are evaluated, along with the improved torque ripple under filleting of stator geometry for 2D model. All results are obtained through simulations.

A. 2D and 3D Model Analysis using FEA

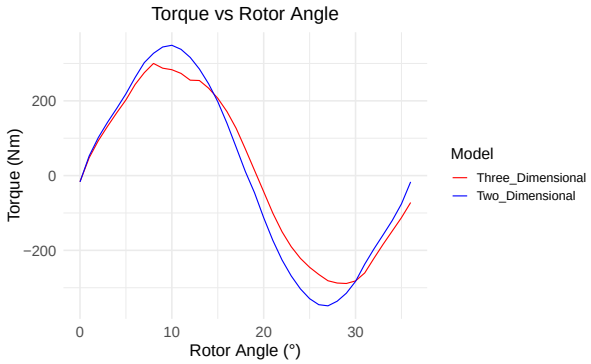

Fig. 5. Torque versus rotor position for 2D and 3D model

1) Static Torque: Fig. 5 shows the torque variation across different rotor positions for the designed DSSRM in 2D and 3D models. The torque waveform reveals a sinusoidal pattern as the rotor position ranges from 0° to 36°, with two different peak torques of 348.76 Nm at 10° for 2D analysis and 300.1 Nm at 8° for 3D analysis.

From the overall waveform of the torque, the peak value occurs at the rotor position with the alignment of rotor segment with stator tooth. This alignment creates the most direct path for magnetic flux, with minimum magnetic reluctance and maximum amplitude of magnetic flux. Moreover, at this point, the reluctance torque is maximised, allowing a greater conversion of electrical input into useful mechanical torque.

However, the comparison reveals differences in the magnetic torque between 2D and 3D analyses. This discrepancy can be attributed to magnetic flux leakage with 3D end effect, which is most significant when the rotor segment is aligned

with the stator tooth. This has been verified with the flux line distribution with 3D FEA, as a significant amount of flux lines are circulating through motor end. The primary factor causing this phenomenon is the effect of magnetic saturation. When the rotor segment is aligned with the stator tooth, the flux density is maximized as the magnetic flux in the air gap interacts with the inner and outer stators, resulting in a substantial portion of magnetic flux being expelled. The stator and rotor cores are working along the non-linear saturation region with significant reluctance. As a result, the flux lines under the 2D main path are limited and further flux lines travel through 3D end, leading to magnetic leakage.

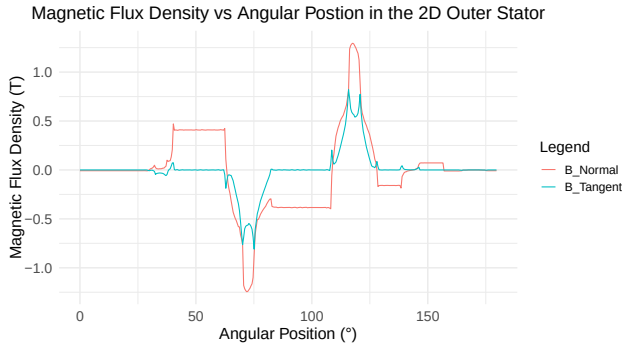

(a) Outer Air-gap

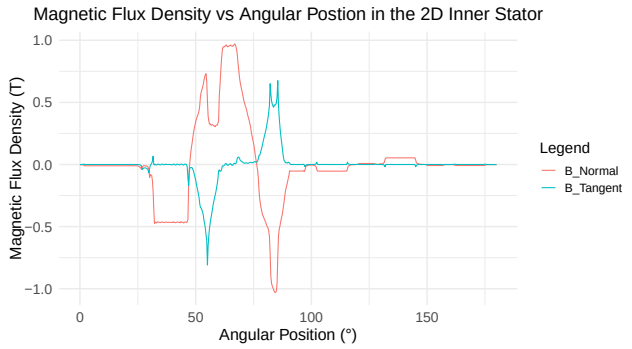

(b) Inner Air-gap

Fig. 6. Stator air-gap flux densities with 2D FEA

2) Outer and Inner Stator Air-gap Flux Density: Fig. 6 and Fig. 7 illustrate that air-gap flux density with 2D and 3D FEA of the DSSRM, highlighting the energy conversion between the outer stator, inner stator, and the rotor. The proximity between the rotors and stators is reduced during the rotation of rotor which allows for the intensity of the magnetic field in the air gap to increase. As the rotor segment is aligned with the stator tooth, an increase in normal magnetic flux density at the rotor's leading edge boosts torque production. A smaller peak in flux density as the rotor exits alignment exerts a minor normal force on the trailing edge, opposing motion. Tangential flux density directly influences torque, with higher densities producing greater tangential forces, as outlined in (2a). Fig. 6 and Fig. 7 indicate how these flux densities counteract each other at alignment, minimising normal force as seen in (2b), with only normal flux density significant around the alignment

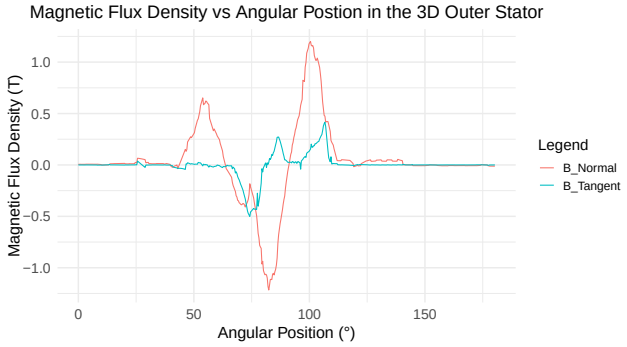

(a) Outer Air-gap

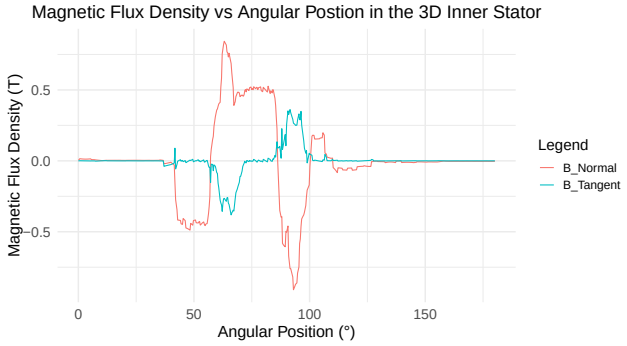

(b) Inner Air-gap

Fig. 7. Stator air-gap flux densities with 3D FEA

phase. Whilst the flux density waveforms are similar with inner air-gap and outer air-gap, the most noticeable difference can be observed as the normal magnetic flux density in the air gap of the outer stator. The difference in magnetic flux density with 3D FEA is influenced by coil configurations and their end windings, which increase resistance and reduce coil currents, thus decreasing magnetic flux density. Eddy currents induced by magnetic leakage in conductive components create opposing magnetic fields, lowering local flux density, and contributing to saturation, limiting flux density growth.

B. Magnetic Flux Density Distribution

Fig. 8 and Fig. 9 demonstrate the 2D and 3D magnetic flux density distribution under a 20 $\mathrm{A\,mm^{-2}}$ excitation current in the various rotor positions, highlighting high flux areas at the stator and rotor teeth and illustrating the flux path from the exciting rotor to the two auxiliary stators. It also depicts the change in flux densities witness throughout the stators as the rotor aligns and moves towards and unaligned position depicting the electromagnetic behaviour of the machine.

The peak flux density is observed at the tips of both stator and rotor cores, which is attributed to the deliberate geometric design aimed at directing magnetic flux towards the air gap. Consequently, magnetic flux lines converge at the narrowest juncture of the gap—located at the tips. This concentration is key to torque generation, inducing a stronger magnetic field that interacts with the rotor to cause rotation.

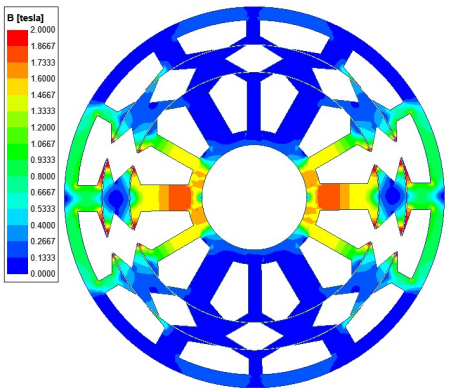

Fig. 8. 2D Magnetic flux density distribution (rotor aligned position)

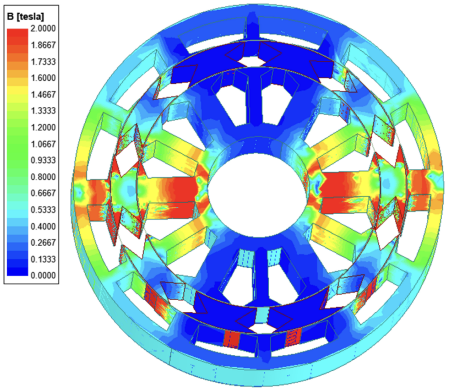

Fig. 9. Magnetic flux density distribution for the 3D model

C. Improved Results Using 2D FEA

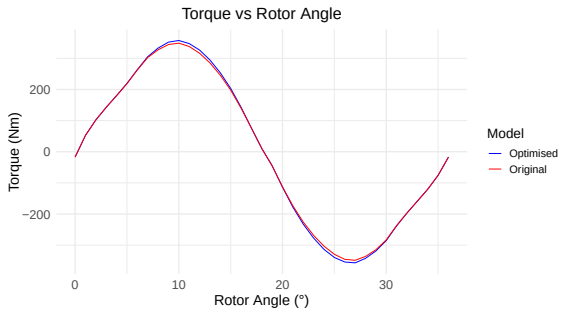

Fig. 10. Static torque waveforms with original and optimised designs

1) Filleted Geometry Design: Fig. 10 shows static torque versus rotor position for the original and improved models with filleted edges, highlighting the optimised model has superior torque performance. The peak torque of the original design is 348.76 Nm, whereas the optimised machine has a peak torque of 357.2 Nm, with an improvement of 2.36%. The improved motor exhibits higher peak torque and a consistent increase in torque throughout its rotation range. Total torque is increased due to the design improvement of rounded edges that optimise flux distribution and the motor's electromagnetic efficiency.

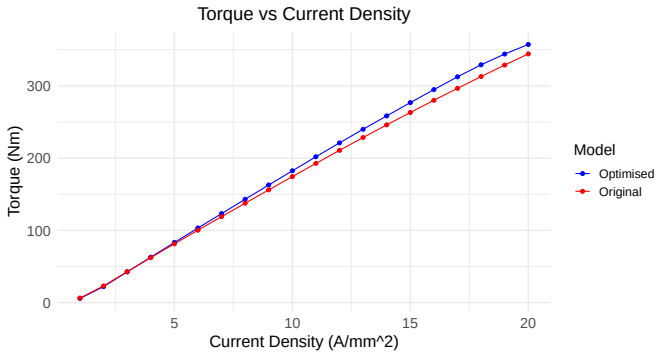

Fig. 11. Peak torque variation with current density of original and improved designs

Fig. 11 displays the peak torque-current density relationship for the original and optimised models. The peak torques are similar at low current densities. As current density rises from 8 A/mm^2 to 18 A/mm^2, the optimised model shows a significantly greater torque increase compared to the original, which explains that the optimised model converts electrical to mechanical energy more efficiently, particularly at medium current densities. As a result, both models perform similarly under low current loads, but the optimised model shows better efficiency under higher loads.

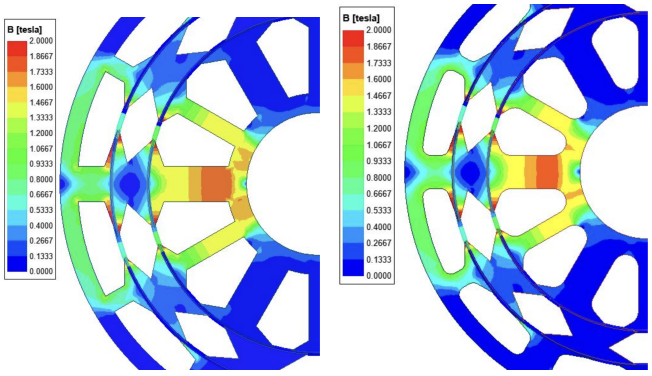

(a) Original (b) Improved

Fig. 12. Magnetic flux density distributions

Analysis of Fig. 12b depicts the improved model has more focused magnetic flux at the stator teeth, and more uniform magnetic flux density thus reducing the iron and heat loss. This flux concentration at the teeth and stators indicates a design optimisation for better magnetic force channelling.

2) Rotor Segment Shift Optimisation: Figs. 13, 14 and 15 illustrate the torque-rotor position relationship, torque ripple, and average torque ripple with rotor segment shifts ranging (δ) from 0° to 4°. The optimal performance is obtained with rotor shift angle of $\delta = 1°$. Whilst the average torque is sacrificed with 0.9%, there is a significant reduction of 9% in torque ripple, as shown in Fig. 15. This also generates a smoother torque profile by effectively reducing the severity of the dip between the commutation of the phases, seen in Fig. 13.

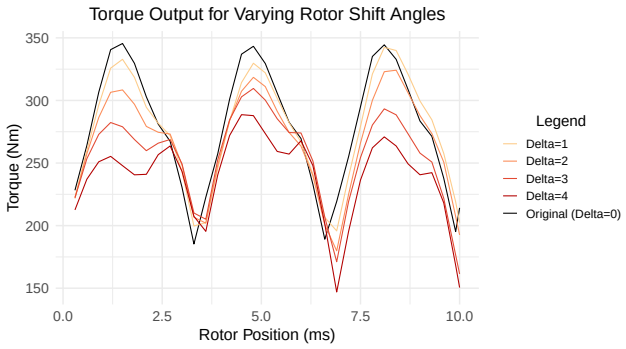

Fig. 13. Electromagnetic torque waveform with the shift of the rotor segments

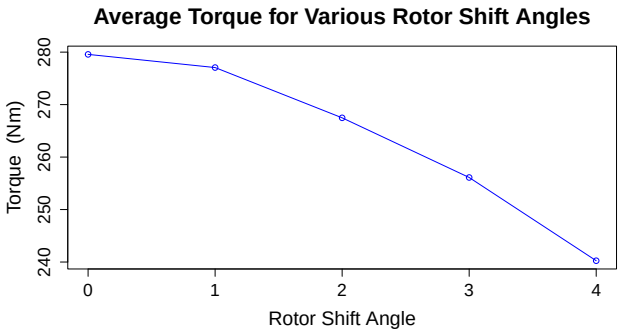

Fig. 14. Average torque versus rotor shift angle

Equation (1a) describes the relationship between inductance variation rate with torque production, highlighting the role of aligned and misaligned inductances. Aligned inductance occurs with stator-rotor alignment, minimising the magnetic flux travelling length in the air gap and magnetic reluctance, thus maximising inductance. Misaligned inductance arises from stator-rotor offset, increasing the air gap and lowering inductance. Increasing the displacement angle δ raises misaligned inductance and its rate of change ($dL/d\theta$) in unaligned positions, while decreasing them in aligned positions, indicating that δ adjustments can alter the inductance change rate during commutation.

TABLE II
PERFORMANCE COMPARISON BETWEEN TWO DSSRMS

Parameter	Original	Optimised
Copper mass (kg)	11.96	11.96
Electrical steel mass (kg)	21.07	21.07
Mass of active parts (kg)	33.03	33.03
Volume (L)	8.6	8.6
Torque ripple (%)	54	44.8
Torque density (Nm/kg)	10.55	10.36
Torque density (Nm/L)	40.47	39.80
Power density (KW/kg)	2.43	2.39
Power density (KW/L)	9.34	9.1

IV. CONCLUSION

In this study, two structural optimisation methods for DSSRM are employed, filleting and rotor segment shift. The

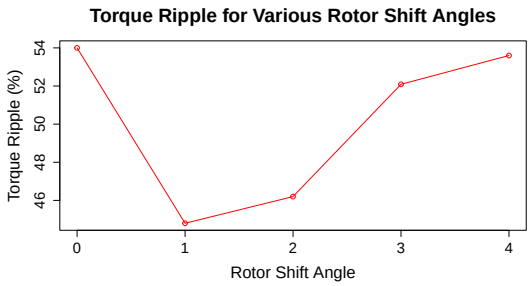

Fig. 15. Torque ripple versus rotor shift angle

implementation of these techniques is presented and 2D and 3D models are further developed for both structures. The electromagnetic performances of these models are evaluated using ANSYS Maxwell. Comparing the performance of the 2D and 3D models, it is observed that the 3D FEA results exhibit slight weakening performance due to end effect. However, it's noted that the 3D model closely mirrors practical motor performance, indicating its relevance despite the performance disparity. The filleting approach yields a notable increase in DSSRM torque, with a recorded improvement of 2.36%. Implementing rotor segment shift reduces torque ripple by about 9%, but only marginally affects overall torque, reducing it by 0.9%. These findings demonstrate the effectiveness of filleting and rotor segment shift in optimising DSSRM performance, particularly in torque and torque ripple.

REFERENCES

[1] C. Lin, W. Wang, and B. Fahimi, "Optimal design of double stator switched reluctance machine (dssrm)," in *2012 IEEE International Symposium on Industrial Electronics*, May 2012.

[2] C.-Y. Wu and C. Pollock, "Analysis and reduction of vibration and acoustic noise in the switched reluctance drive," *IEEE Transactions on Industry Applications*, vol. 31, no. 1, pp. 91–98, January-February 1995.

[3] D. E. Cameron, J. H. Lang, and S. D. Umans, "The origin and reduction of acoustic noise in doubly salient variable-reluctance motors," *IEEE Transactions on Industry Applications*, vol. 28, no. 6, pp. 1250–1255, November-December 1992.

[4] e. a. Maharjan, "Comprehensive report on design and development of a 100-kw dssrm," *IEEE Transactions on Transportation Electrification*, vol. 4, no. 4, pp. 835–856, December 2018.

[5] T. D. Gupta, K. Chaudhary, R. M. Elavarasan, R. K. Saket, I. Khan, and E. Hossain, "Design modification in single-tooth winding double-stator switched reluctance motor for torque ripple mitigation," *IEEE Access*, vol. 9, pp. 19 078–19 096, 2021.

[6] M. Abbasian, M. Moallem, and B. Fahimi, "Double-stator switched reluctance machines (dssrm): Fundamentals and magnetic force analysis," *IEEE Transactions on Energy Conversion*, vol. 25, no. 3, pp. 589–597, September 2010.

[7] N. Neupane, "Comparison of switched reluctance motor and double stator switched reluctance motor," 2018, accessed: Mar. 18, 2024.

[8] W. Yan, H. Chen, Y. Liu, H. Cheng, and M. Orabi, "A magnetic field decoupling double stator switched reluctance machine," *IEEE Transactions on Applied Superconductivity*, vol. 31, no. 8, pp. 1–5, November 2021.

[9] E. Bostanci, M. Moallem, A. Parsapour, and B. Fahimi, "Opportunities and challenges of switched reluctance motor drives for electric propulsion: A comparative study," *IEEE Transactions on Transportation Electrification*, vol. 3, no. 1, pp. 58–75, March 2017.

[10] B. Mecrow, "Fully pitched-winding switched-reluctance and stepping-motor arrangements," *IEE Proceedings B-Electric Power Applications*, vol. 140, no. 1, pp. 61–61, Jan. 1993.